Cavity quantum electrodynamics with quantum dots in microcavities

Gudat, J.

Chapter 6

Spin Quantum Jumps

This chapter is published in *Spin quantum jumps in a singly charged quantum dot* (M. P. van Exter, J. Gudat, G. Nienhuis, and D. Bouwmeester, Phys. Rev. A 80, 023812 (2009)) [129].

This chapter presents a theoretical model of the spin dynamics of a confined electron spin in a quantum dot embedded in a micro pillar cavity. There will be four levels involved in the dynamics; two ground states that correspond to the electron spin of $\pm\frac{1}{2}$ and two excited states that correspond to two trion states with total spin $\pm\frac{3}{2}$. Under the influence of driving electromagnetic fields (these could be the intra-cavity fields or external laser fields) there will be coherent (Rabi type) transitions between levels. Furthermore we have to treat the four-level system as an open quantum system in order to include dissipative processes, such as spontaneous emission of photons or coupling to phonons, which lead to decay of the excited states and to incoherent couplings between the two excited states and between the two ground states. The investigation of open quantum systems in quantum optics requires the introduction of the Master equation for the reduced density operator of the system of interest.

The time evolution of the reduced density operator describes the ensemble averaged dynamics of the system of interest and therefore leads to a smooth evolution of all level populations and coherences involved. The simplest example is spontaneous emission from a two-level atom which leads to exponential decay of the excited state population into the ground state population. In order to verify this dynamics we have to average over an ensemble of realizations of this two-level system. A natural question to ask is what happens for each individual member of the ensemble. Experimentally we measure no smooth decay for a single system but we typically observe an abrupt quantum jump at a

largely random moment in time characterized by the emission and subsequent detection of a photon. Niels Bohr described the notion of quantum jumps in his early work in 1913 [130] and referred to them as a crucial step forward in the understanding of atoms. Schrödinger completed the Bohr picture of atoms when introducing the theory of quantum mechanics in 1926 [131]. The Schrödinger equation allows determining the discrete energy level structure of an atom and also the transition rates associated with the quantum jumps.

Detecting the emission of a single photon from a single atom in an efficient way is technically very challenging. Therefore, the concept of quantum jumps is often discussed in the context of a three-level system [132] by which a ground state is coupled by one strong (ω_1) and one weak (ω_2) laser field to two excited states. The strong field is often referred to as the cycling field and provides an easily detectable photon flux at frequency ω_1 provided the system is not *shelved* into the other excited state. The abruptly turning on and off at random times (often referred to as a telegraph signal) of the fluorescence at ω_1 is a proof for the occurrence of quantum jumps. The aim of this chapter is to predict the quantum jump statistics between spin states of a confined electron in a quantum dot. Understanding the spin jump statistics requires detailed knowledge of the various processes that influence the electron spin. Therefore comparing theory with experiments will help us improving our understanding of the electron spin dynamics.

The analysis of open quantum systems can quickly get rather complicated if several interactions are contributing to the dynamics. In such cases it can be very advantageous to break the dynamics down into fast and slow motion. The fast dynamics will lead to quasi-stationary states, while the slow dynamics will lead to transitions between those states on slow time scales. The general principal of this separation of fast and slow variables has been developed by Nienhuis [133]; in this chapter it will be applied to the four-level system of interest.

Before addressing the four-level quantum dot system (Sect. 6.3), we will briefly review some of the elementary tools of quantum open systems (Sect.6.1) and give an introduction to the technique of separation of time scales (Sect.6.2).

6.1 Open quantum systems

We first briefly review properties of the density operator. The discussion is followed by introducing the Liouville operator which describes the time evo-

lution of the density matrix of a quantum mechanical system. It contains the Hamiltonian operator which determines the time evolution of the quantum state vector. The way a Hamiltonian determines the evolution of a state vector, the Liouville operator determines the evolution of the density matrix. By means of an example for a two-level system we explain how we will treat dissipation of energy mathematically by using the master equation for open quantum systems.

6.1.1 Density operator

Quantum states described by state vectors are *pure* states. If the available information is not sufficient to determine the *pure* state vector we can describe a subsystem of the full system by a *mixed* state using the density operator

$$\hat{\rho} = \sum_i \mid \psi_i\rangle p_i \langle\psi_i \mid, \tag{6.1}$$

where the sum is over an statistical ensemble with p_i the probability of the subsystem being in the i-th state of the ensemble $\mid \psi_i\rangle$. The *mixed* state contains no information on possible correlations between states $\mid \psi_i\rangle$ and $\mid \psi_j\rangle$, with $i \neq j$. It is of course possible to describe a *pure* state with a density matrix by simply having $p_i = 1$ for the state $\mid \psi_i\rangle$. For a complete orthonormal basis $\{\mid \varphi_n\rangle\}$, where $\sum_n \mid \varphi_n\rangle\langle\varphi_n \mid = \hat{I}$, of eigenstates of some observer, the density matrix can be described by its density matrix elements with respect to this basis

$$\begin{aligned} \hat{\rho}_{nn'} &= \langle\varphi_n \mid \hat{\rho} \mid \varphi_{n'}\rangle & (6.2)\\ &= \sum_i \langle\varphi_n \mid \psi_i\rangle p_i \langle\psi_i \mid \varphi_{n'}\rangle & (6.3)\\ &= \sum_i p_i c_n^{(i)} c_{n'}^{(i)} * & (6.4) \end{aligned}$$

As a simple example consider a two-level system with an excited state $\mid e\rangle$ and a ground state $\mid g\rangle$. Consider the state $\mid \psi\rangle = \frac{1}{\sqrt{2}}(\mid e\rangle + e^{i\phi} \mid g\rangle)$ with ϕ describing the phase relation between $\mid e\rangle$ and $\mid g\rangle$. This coherent superposition state is a pure state. The density operator is given by

$$\hat{\rho} = \mid \psi\rangle\langle\psi \mid = \frac{1}{2}\left(\mid e\rangle\langle e \mid + \mid g\rangle\langle g \mid + e^{i\phi} \mid g\rangle\langle e \mid + e^{-i\phi} \mid e\rangle\langle g \mid\right). \tag{6.5}$$

The density matrix elements are $\hat{\rho}_{ee} = \frac{1}{2}$, $\hat{\rho}_{eg} = \frac{e^{-i\phi}}{2}$, $\hat{\rho}_{ge} = \frac{e^{i\phi}}{2}$ and $\hat{\rho}_{gg} = \frac{1}{2}$. A criterion for determining whether a density matrix describes a pure or a mixed state is

$$Tr\hat{\rho}^2 = Tr\hat{\rho} = 1, \tag{6.6}$$

for a pure state (as is the case for (6.5)) and $Tr\hat{\rho}^2 < Tr\hat{\rho} = 1$ for a mixed state. Consider for example the mixed state given by

$$\hat{\rho}_{mixed} = \frac{1}{2}\left(|\, e\rangle\langle e\,| + |\, g\rangle\langle g\,|\right). \tag{6.7}$$

This state cannot be expressed by a state vector and has $Tr\hat{\rho}^2_{mixed} = 1/2$.

6.1.2 Liouville operator

The coherent evolution of the density matrix is described by a unitary operator $\hat{U}$:

$$\hat{\rho} = \sum_i p_i |\psi_i\rangle\langle\psi_i| \rightarrow \sum_i p_i \hat{U}|\psi_i\rangle\langle\psi_i|\hat{U}^\dagger = \hat{U}\hat{\rho}\hat{U}^\dagger. \tag{6.8}$$

The time derivative of $\hat{\rho}(t)$ is given by

$$\frac{\partial\hat{\rho}}{\partial t} = \sum_i p_i \left[\left(\frac{\partial}{\partial t}|\psi_i(t)\rangle\right)\langle\psi_i(t)| + |\psi_i(t)\rangle\left(\frac{\partial}{\partial t}\langle\psi_i(t)|\right)\right]. \tag{6.9}$$

According to the Schrödinger equation for the bra state vector $\langle\psi_i(t)|$ we can write

$$-i\hbar\frac{\partial}{\partial t}\langle\psi_i(t)| = \langle\psi_i(t)|\hat{H}^\dagger. \tag{6.10}$$

Therewith it follows

$$\begin{aligned}\frac{\partial\hat{\rho}}{\partial t} &= \frac{1}{i\hbar}\sum_i p_i\left[\left(\hat{H}|\psi_i(t)\rangle\right)\langle\psi_i(t)| - |\psi_i(t)\rangle\left(\langle\psi_i(t)|\hat{H}^\dagger\right)\right] \\ &= \frac{1}{i\hbar}(\hat{H}\hat{\rho} - \hat{\rho}\hat{H}^\dagger) = \frac{1}{i\hbar}[\hat{H},\hat{\rho}].\end{aligned} \tag{6.11}$$

In the last step we assumed $\hat{H} = \hat{H}^\dagger$, in other words the Hamiltonian has real eigenvalues. The general solution of Eq. (6.11) is given by

$$\hat{\rho}(t) = e^{-i\hat{H}t/\hbar}\hat{\rho}(0)e^{i\hat{H}t/\hbar} \tag{6.12}$$

$$= \hat{U}(t)\hat{\rho}(0)\hat{U}^\dagger(t) \tag{6.13}$$

which brings us back to the Unitary operator $\hat{U}$ and the same form we introduced in Eq.(6.8). Now we can express the equation of motion for $\hat{\rho}(t)$ with the **Liouville operator** $\mathcal{L}$

$$\mathcal{L} = \frac{1}{i\hbar}[\hat{H},...] \tag{6.14}$$

where $\hat{\rho}(t)$ satisfies

$$\frac{\partial \hat{\rho}}{\partial t} = \mathcal{L}\hat{\rho}, \tag{6.15}$$

with the formal solution

$$\hat{\rho}(t) = e^{\mathcal{L}t}\hat{\rho}(0). \tag{6.16}$$

In dissipative processes part of the Hamiltonian can be non-Hermitian, i.e. not norm preserving and Eq. (6.14) has to be augmented with additional terms outside the commutator $[\hat{H}, ...]$ leading to the master equation for open systems. This will be discussed in the next section.

6.1.3 Master equation

By dissipative processes we mean transitions between states that take place by irreversible emission of energy into the surrounding environment (often in the form of a photon or phonon). Since we typically cannot have full knowledge of the state of the environment we loose information about the system of interest (for example a two-level atom) that interacts with the environment (for example a bath of electromagnetic modes).

There are several methods to arrive at the so-called master equation for the reduced density matrix for the system of interest. For the generic case of a two-level atom driven by a laser field with a detuning $\delta = \omega_{laser} - \omega_{atom}$ and undergoing spontaneous emission corresponding to a decay rate Γ of the excited state population to the ground state the master equation is of the form:

$$\frac{d\hat{\rho}}{dt} = \frac{i}{\hbar}\left[\hat{\rho}, \hat{H}_0\right] - \frac{\Gamma}{2}\left(\hat{S}^+\hat{S}^-\hat{\rho} + \hat{\rho}\hat{S}^+\hat{S}^- + 2\hat{S}^-\hat{\rho}\hat{S}^+\right), \tag{6.17}$$

where $\hat{S}^+ =\mid e\rangle\langle g \mid$ and $\hat{S}^- =\mid g\rangle\langle e \mid$.

The coherent dynamics as a result of a classical driving field $E(t) = E_0 \cdot \cos(\omega_{laser}t)$ is included in $\hat{H}_0 = -\delta\hat{S}^+\hat{S}^- + \frac{\Omega}{2}(\hat{S}^+ + \hat{S}^-)$ with $\Omega = -dE_0$, the Rabi frequency, with d the atomic dipole moment.

The incoherent dynamics as the result of dissipation is described by the $-\Gamma\hat{S}^-\hat{\rho}\hat{S}^+$ term. Written out as $-\Gamma \mid g\rangle\langle e \mid \hat{\rho} \mid e\rangle\langle g \mid$ this term has the clear interpretation of reducing the population in the excited state by going to the ground state with a rate at time t of $\Gamma|\alpha_e(t)|^2$, with $|\alpha_e(t)|^2$ the probability to be in the excited state at time t.
The other two terms $-\frac{\Gamma}{2}\hat{S}^+\hat{S}^-\hat{\rho}$ and $-\frac{\Gamma}{2}\hat{\rho}\hat{S}^+\hat{S}^-$ can be interpreted as resulting from a non-Hermitian (i.e. non normpreserving) part of the Hamiltonian

$\frac{i\hbar\Gamma\hat{S}^{+}\hat{S}^{-}}{2}$ that acts in periods of no emission of a photon in a single quantum trajectory [134, 135]. The terms indicate loss of the excited state population which, after the renormalization that needed to correct for the non-Hermitian nature of part of the Hamiltonian, automatically leads to an increase of the ground state population. There are at least two ways to interpret this part of the evolution. The first is that in a period dt in which no emission of a photon is observed, we do obtain information about the system that indicates that the system is more likely to be in the ground state at the end of period dt than at the beginning. The second way is to investigate a full quantum electrodynamics derivation of the interaction of the atom with the radiation field [135]. It will be clear that if a photon can be spontaneously emitted there will also be a second order process by which a photon will be emitted and reabsorbed. This process of radiation reaction will precisely describe the decay from excited to ground state (without permanently emitting a photon) together with an energy shift of the excited state relative to the ground state (this energy shift is assumed to be already accounted for in the atomic transition frequency ω_{atom}).
Note that one naively would think that this second order process of radiation reaction would have a neglectable effect compared to the first order process of emission. This is however not the case since radiation reaction brings the atomic system back to the initial state and therefore interference takes place between no emission (the $\hat{I}$) operator and radiation reaction described by H_{int}^2. Taking the square of the sum of amplitudes $(\hat{I} + \hat{H}_{int}^2)^2$ results in the same order in change of state as resulting from $(\hat{H}_{int})^2$ for the emission probability of permanent emission of a photon.)
The general form Eq.(6.17) will play a central role in formulating our four-level mode for a singly charged quantum dot in a micropillar cavity.

6.2 Separation of time scales

As will be shown in Sect. 6.3 our single charged quantum dot system can be modeled by a 4-level system with various optical and nonradiative interactions between the levels. Using the mathematical method of separating slow and fast dynamics of our multi-state system will be crucial for computing the evolution of the system. Doing this we can ease the mathematical computation and extract separate physical properties of the system. This idea is based on earlier work of Nienhuis [133].

As introduced in Sect. 6.1.2 the statistical properties and averaged dynamics of our system is described by the density matrix operator $\hat{\rho}(t)$ and

$$\frac{d}{dt}\hat{\rho}(t) = \mathcal{L}\hat{\rho}(t), \tag{6.18}$$

where the Liouville operator $\mathcal{L}$ contains the coupling to the external radiative field, the spontaneous decay and nonradiative couplings between levels. Acting on the density matrix $\hat{\rho}$ it leads to complex results making it very difficult to derive general solutions for (6.18). Fortunately we are not interested in the complete evolution of the density matrix $\hat{\rho}(t)$ but only in a few aspects of the evolution that provides information about the outcomes of the specific measurements performed on the system (such as detecting photon emission). This allows for separating $\mathcal{L}$ into two (or more) terms

$$\mathcal{L} = \mathcal{L}_0 + \mathcal{L}_1 \tag{6.19}$$

leading to reduced evolution equations. The idea of this approach is to physically separate between the effects that cause a fast and a slow evolution of the system. We take $\mathcal{L}_0$ to describe a much more rapid evolution as compared to $\mathcal{L}_1$. This means that on a rapid time scale the system is driven to a *stationary solution* by $\mathcal{L}_0$ when completely neglecting $\mathcal{L}_1$.

$$\frac{d}{dt}\hat{\rho}(t) = \mathcal{L}_0\hat{\rho}(t) \tag{6.20}$$

Given this stationary solution, the time derivation of the density matrix $\hat{\rho}(t)$ equals zero. In other words, the stationary solution lies within the subspace of the matrices $\hat{\rho}$ that are eigenvectors of $\mathcal{L}_0$ with eigenvalue zero.

The role of $\mathcal{L}_1$ is to introduce transitions between the (quasi) stationary solutions of (6.20). To separate the dynamics resulting from the fast and slow dynamics we introduce the linear projector $\hat{\mathcal{P}}$ and its complement

$$\hat{\mathcal{Q}} = 1 - \hat{\mathcal{P}}. \tag{6.21}$$

$\hat{\mathcal{P}}$ projects any matrix $\hat{\rho}$ onto the subspace of the stationary solutions explained in (6.20). $\hat{\mathcal{P}}$ and $\hat{\mathcal{Q}}$ both obey the projector equality

$$\hat{\mathcal{P}}^2 = \hat{\mathcal{P}} \tag{6.22}$$

$$\hat{\mathcal{Q}}^2 = \hat{\mathcal{Q}} \tag{6.23}$$

Additionally $\hat{\mathcal{P}}$ is defined to project onto the subspace of eigenvectors of $\mathcal{L}_0$ with eigenvalue zero

$$\mathcal{L}_0\hat{\mathcal{P}} = \hat{\mathcal{P}}\mathcal{L}_0. \tag{6.24}$$

Now, on the rapid time scale we assume that the evolution operator $\mathcal{L}_0$ drives every initial density matrix $\hat{\rho}$ to its projection $\hat{\mathcal{P}}\hat{\rho}$. This implies that $\hat{\mathcal{P}}$ leaves invariant all eigenvectors of $\mathcal{L}_0$ with eigenvalue zero. Additionally we know that all non-zero eigenvalues of $\mathcal{L}_0$ have a negative imaginary part, in other words the corresponding eigenstates will decay over time. Therefore we can write

$$e^{\mathcal{L}_0\tau} \to \hat{\mathcal{P}}\hat{\rho}. \tag{6.25}$$

for a large τ on the rapid time scale.

We can now derive a pair of coupled equations for the two projections $\hat{\mathcal{P}}$ and $\hat{\mathcal{Q}}$ of $\hat{\rho}$ from formula (6.18) and (6.19) using (6.21) and (6.24).

$$\frac{d}{dt}\hat{\mathcal{P}}\hat{\rho} = \hat{\mathcal{P}}\mathcal{L}\hat{\rho} = \hat{\mathcal{P}}\mathcal{L}_1\hat{\mathcal{P}}\hat{\rho} + \hat{\mathcal{P}}\mathcal{L}_1\hat{\mathcal{Q}}\hat{\rho}. \tag{6.26}$$

$$\frac{d}{dt}\hat{\mathcal{Q}}\hat{\rho} = \hat{\mathcal{Q}}\mathcal{L}\hat{\rho} = \hat{\mathcal{Q}}(\mathcal{L}_0 + \mathcal{L}_1)\hat{\mathcal{Q}}\hat{\rho} + \hat{\mathcal{Q}}\mathcal{L}_1\hat{\mathcal{P}}\hat{\rho}. \tag{6.27}$$

The last expression consists of two components, a sort of damping term $\hat{\mathcal{Q}}(\mathcal{L}_0 + \mathcal{L}_1)\hat{\mathcal{Q}}\hat{\rho}$ and a driving term $\hat{\mathcal{Q}}\mathcal{L}_1\hat{\mathcal{P}}\hat{\rho}$. We want to find a formal solution for $\hat{\mathcal{Q}}\hat{\rho}(t)$ (Eq. (6.27)) in order to insert this into Eq. (6.26) to find the time evolution of $\hat{\mathcal{P}}\hat{\rho}(t)$. In order to do so we define

$$X(t) \widehat{=} e^{-\hat{\mathcal{Q}}(\mathcal{L}_0+\mathcal{L}_1)\hat{\mathcal{Q}}t}\hat{\mathcal{Q}}\hat{\rho}(t). \tag{6.28}$$

Time derivation leads to

$$\frac{d}{dt}X(t) = -\hat{\mathcal{Q}}(\mathcal{L}_0 + \mathcal{L}_1)\hat{\mathcal{Q}}e^{-\hat{\mathcal{Q}}(\mathcal{L}_0+\mathcal{L}_1)\hat{\mathcal{Q}}t}\hat{\mathcal{Q}}\hat{\rho}(t) + e^{-\hat{\mathcal{Q}}(\mathcal{L}_0+\mathcal{L}_1)\hat{\mathcal{Q}}t}\frac{d\hat{\mathcal{Q}}\hat{\rho}(t)}{dt}. \tag{6.29}$$

This can be rewritten as

$$\frac{d}{dt}\hat{\mathcal{Q}}\hat{\rho}(t) = e^{\hat{\mathcal{Q}}(\mathcal{L}_0+\mathcal{L}_1)\hat{\mathcal{Q}}t}\frac{dX}{dt} + \hat{\mathcal{Q}}(\mathcal{L}_0 + \mathcal{L}_1)\hat{\mathcal{Q}}\hat{\rho}(t) \tag{6.30}$$

where the first term compares to the driving term in Eq. (6.27). We can therefore write

$$\frac{d}{dt}X(t) = e^{-\hat{\mathcal{Q}}(\mathcal{L}_0+\mathcal{L}_1)\hat{\mathcal{Q}}t}\hat{\mathcal{Q}}\mathcal{L}_1\hat{\mathcal{P}}\hat{\rho}(t). \tag{6.31}$$

This term can be formally integrated and together with (6.28) yields

$$\hat{\mathcal{Q}}\hat{\rho}(t) = \int_0^\infty e^{\hat{\mathcal{Q}}(\mathcal{L}_0+\mathcal{L}_1)\hat{\mathcal{Q}}\tau}\hat{\mathcal{Q}}\mathcal{L}_1\hat{\mathcal{P}}\hat{\rho}(t-\tau)d\tau. \tag{6.32}$$

Using relation (6.21) and equality (6.24) we can derive a simpler expression for part of the exponent of (6.32)

$$\begin{aligned}\hat{\mathcal{Q}}\mathcal{L}_0\hat{\mathcal{Q}} &= (1-\hat{\mathcal{P}})\mathcal{L}_0(1-\hat{\mathcal{P}}) \\ &= \mathcal{L}_0 - \hat{\mathcal{P}}\mathcal{L}_0 - \mathcal{L}_0\hat{\mathcal{P}} + \hat{\mathcal{P}}^2\mathcal{L}_0 = \mathcal{L}_0 + \hat{\mathcal{P}}^2\mathcal{L}_0 \\ &= \mathcal{L}_0 + \hat{\mathcal{P}}\mathcal{L}_0 = \mathcal{L}_0 \end{aligned} \tag{6.33}$$

Since our aim is to derive an expression for an approximate solution of the time evolution of $\hat{\mathcal{P}}\hat{\rho}(t)$ by inserting (6.32) into (6.26) we restrict ourselves to the first-order contribution of (6.32). This allows us to neglect $\hat{\mathcal{Q}}\mathcal{L}_1\hat{\mathcal{Q}}\tau$ compared to $\mathcal{L}_0\tau$ in the exponent. Additionally we treat the time dependance of $\hat{\mathcal{P}}\hat{\rho}(t-\tau)$ to zeroth-order resulting in $\hat{\mathcal{P}}\hat{\rho}(t)$ (the exponent $e^{\mathcal{L}_0 t}$ will dominate the τ dependance). Identity (6.32) thus simplifies to

$$\hat{\mathcal{Q}}\hat{\rho}(t) = \int_0^\infty e^{\mathcal{L}_0\tau}\hat{\mathcal{Q}}\mathcal{L}_1\hat{\mathcal{P}}\hat{\rho}(t)d\tau. \tag{6.34}$$

In continuation of the discussion explaining why Eq. (6.25) is justified in this context, we know that the integrant with the exponential $e^{\mathcal{L}_0\tau}$ goes to zero on the rapid time scale so that an integral converges. This leads us to the following approximate expression for the time evolution of $\hat{\mathcal{P}}\hat{\rho}(t)$ that is at the same time the starting point for our analysis of the four-level system explained in the next section:

$$\frac{d}{dt}\hat{\mathcal{P}}\hat{\rho}(t) = \hat{\mathcal{P}}\mathcal{L}_1\hat{\mathcal{P}}\hat{\rho}(t) + \hat{\mathcal{P}}\mathcal{L}_1\int_0^\infty e^{\mathcal{L}_0\tau}\hat{\mathcal{Q}}\mathcal{L}_1\hat{\mathcal{P}}\hat{\rho}(t)d\tau. \tag{6.35}$$

6.3 Spin quantum jumps in a singly charged quantum dot

The spin of a single charge confined to an optically active QD can serve as a solid-state quantum bit [136–138]. The charge confinement leads to discrete energy levels that quenches the electron spin relaxation [139] compared to relaxation in bulk (or quantum well) structures where there is a quasi continuum of states. Therefore the QD confined electron spin can exhibit long spin relaxation times and a long lived coherence between its two ground states. Long lifetimes in excess of $\approx 1\mu s$ are expected [140] compared to optical interactions with the spin on time scales of sub 1ns. Experimental realization can be achieved by electrically addressing a single-electron charged QD in a high-finesse microcavity [4,5,56,67,141,142] forming a trion state by addition of an exciton upon optical excitation [55,94]. For quantum-information processing with electron spins it is crucial to read out the state of a single confined spin.

This has been achieved by using the optical read-out techniques based on the Faraday [143] or the Kerr effect [144]. In both cases the read-out was very inefficient. With a single QD in a microcavity we can theoretically change its reflectivity up to 100% [54] by changing the spin state and therewith implement an efficient single-qubit readout. Experimentally we have shown a change of the cavity reflection of 50% [55]. Having control over the polarization properties of the cavity with the technique described in Chap. 4 we aim for switching the reflectivity by more than 90%.

Based on the analysis presented in this chapter, we predict the occurrence of sudden jumps between well defined, approximately stationary, spin states of the QD. This prediction is a generalization of the quantum jumps that are known to occur in three-level systems. The latter jumps were originally proposed by Dehmelt [145], who described them in terms of *electron shelving* from a strong optical (cycling) transition to a weakly interacting level and explained how the statistics of the intermittent fluorescence can be used to analyze weak transitions in single-atom spectroscopy. Cook and Kimble [146] predicted that under continuous incoherent excitation the observed fluorescence should randomly switch *on* and *off*, resulting in a random telegraph signal. First experiments observing quantum jumps were performed with trapped atoms in the 1980's by Wineland *et al.* [147], Bergquist *et al.* [148] and Kimble *et al.* [149]. Quantum jumps in semiconductor structures have first been observed by blinking statistics in single semiconductor nanocrystal QDs by Shimizu *et al.* [150]. A very good review on the different theoretical approaches to describe quantum jump dynamics in quantum optics is given by Plenio and Knight [151].

This section analyzes the optically driven dynamics of a singly charged self-assembled QD modeled as a four-level system. Such four-level systems have been used to describe a variety of phenomena like coherent population trapping, electromagnetically induced transparency and lasing without inversion (see reference [152] and references therein). The ansatz for describing the four-level system in this chapter is to differentiate between its various dynamics allowing to adopt the method for the separation of time scales introduced in the previous section. This is a useful approach because of the relatively fast spontaneous decay from the two upper excited levels to the two lower ground levels which effectively removes most quantum-interference effects. The dynamics are described in terms of effective populations and jump rates.

In this section we first introduce the four-level system before we discuss the separation of time scales discussed in Sect. 6.2. First, relatively simple expressions for the quantum jump rates due to incoherent spin flips are derived. The section is followed by more intricate quantum jumps due to coherent spin coupling. Finally, experimental possibilities are outlined as is a refined model.

6.3.1 The four-level system

Although QD are often referred to as artificial atoms there are large differences in the electron energy level structures compared to free atoms. In particular a QD has a natural quantization axis set by the growth direction and pancake shape compared to the rotationally symmetric free atom. The resulting energy separation between the heavy-hole ($m = \pm\frac{3}{2}$) and the light-hole ($m = \pm\frac{1}{2}$) states allows to experimentally single out the optical transition to the heavy-hole exciton state. Therewith a natural preference for the spin basis can be created. The spontaneous emission from this transition is strongest in the direction of the quantization axis and is circularly polarized in this direction.
Processes included in the QD model are coherent coupling between the electron or hole spin levels due to interaction with the nuclei of the semiconductor host material [153], spontaneous spin flips due to interaction with the phonon bath, and coherent coupling between ground and excited states due to the driving optical field [55]. In our model we assume a constant field-induced coupling described by two fixed Rabi frequencies Ω_+ for right-handed circularly polarized light and Ω_- for left-handed circularly polarized light. This relatively simple and clean case with constant coupling rate is discussed and analyzed in detail. An outline for a refined model that includes back action of the electron spin on the nuclear spin and the intracavity field is presented in Sect. 6.5.

Figure 6.1 introduces the four-level system for a negatively charged quantum dot. It shows the energy levels and the relevant coupling and decay rates between the four states. The model defines the two ground state levels 1 and 3 with a single electron in a quantum dot. The electron can either point up $|\uparrow\rangle$ (state 1) or down $|\downarrow\rangle$ (state 3). The two upper excited-state levels 2 and 4 with a charged exciton (trion) state consist of an electron pair in the singlet state and an additional heavy hole denoted as $|\uparrow\downarrow\Uparrow\rangle$ (state 2) and $|\uparrow\downarrow\Downarrow\rangle$ (state 4). Electron spin neutrality for each of these states is imposed by the Pauli principle (which forbids creation of $|\uparrow\uparrow\Downarrow\rangle$ and $|\downarrow\downarrow\Uparrow\rangle$).

A possible detuning $\delta_3 \equiv \omega_{31} \equiv \omega_3 - \omega_1$ between the two ground states 1 and 3 caused by the out-of-plane component of the (nuclear) magnetic field is also considered. This nuclear magnetic field varies slowly on a typical time scale of micro- to milliseconds, depending on temperature, external field and material composition [154]. Our model treats the variation of this field as quasi-static, i.e. as if the fluctuations are frozen in time [155]. Past fluctuations are experimentally integrated over time and result in an additional decoherence. This is the *pure dephasing* time T_2^* as part of the time-averaged decoherence time T_2. Other frequency splittings considered are $\delta_2 \equiv \omega_{21} - \omega_0$

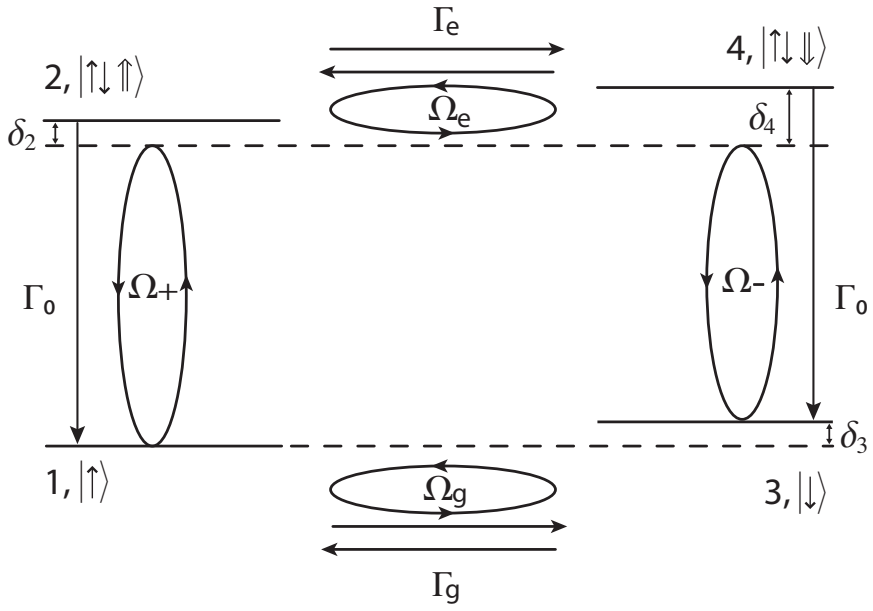

Figure 6.1: *Energy levels and internal dynamics for the four-level system.*

and $\delta_4 \equiv \omega_{41} - \omega_0$, both defined with respect to the optical frequency ω_0 of the optical pump. These splittings depend on the circular anisotropy. Linear anisotropies, caused by mechanical strain and crystal-field effects, are described by a coherent coupling between the spin levels. The exciton fine-structure splitting observed in neutral quantum dots with asymmetric shapes [156] results from spin-orbit coupling. It is absent in singly charged quantum dots [157] because the total electron spin in the singlet state is zero.
Now we express the populations and coherences in this four-level system by the density matrix $\hat{\rho}(t)$ as conceptually introduced in the previous section. $\hat{\rho}(t)$ is a 4×4 matrix. Its evolution is described in a rotating basis with the two upper states rotating at a frequency ω_0 with respect to the two ground states. A crucial aspect for the analysis is the distinction between *spin-conserving transactions* which occur between levels $1 \leftrightarrow 2$ or $3 \leftrightarrow 4$ and *spin-changing transitions* that take place between levels $1 \leftrightarrow 3$ or $2 \leftrightarrow 4$. The model includes ten relevant interactions of which four are coherent couplings and six are decay transitions.

First we describe the coherent interactions which are indicated by closed loops in Fig. 6.1. The optical field creates a coherent coupling between ground

and excited states of equal handedness. Right handed circularly polarized light results in a coherent coupling of the spin-up states (1 and 2) at a frequency $\Omega_{1\leftrightarrow 2} \equiv \Omega_+$ whereas left handed circularly polarized light results in a coherent coupling of the spin-down state (3 and 4) at a frequency $\Omega_{3\leftrightarrow 4} \equiv \Omega_-$. A possible *in-plane* (nuclear) magnetic field, or any other linear anisotropy, will induce a coherent coupling between spin states of opposite handedness. The two ground states are connected via a coherent coupling frequency $\Omega_{1\leftrightarrow 3} \equiv \Omega_g$ while the two excited states are connected via a coupling frequency $\Omega_{2\leftrightarrow 4} \equiv \Omega_e$. The rates Ω_g and Ω_e can differ due to different g factors for electrons and holes. A single Hamiltonian H can describe the coherent coupling frequencies and frequency splittings:

$$H = -\frac{\hbar}{2}\begin{pmatrix} 0 & \Omega_+ & \Omega_g & 0 \\ \Omega_+ & 2\delta_2 & 0 & \Omega_e \\ \Omega_g & 0 & 2\delta_3 & \Omega_- \\ 0 & \Omega_e & \Omega_- & 2\delta_4 \end{pmatrix}. \tag{6.36}$$

The six incoherent interactions in our model are indicated as straight arrows in Fig. 6.1. Spontaneous emission of photons results in population decay from the two excited states (2 and 4) to the associated ground states (1 and 3) at rates $\Gamma_{2\leftarrow 1} = \Gamma_{4\leftarrow 3} \equiv \Gamma_0$. A possible enhancement of the decay rates with respect to the their free-space value is described by the Purcell effect and included in our definition of Γ_0 [55].

The two ground states 1 and 3 are connected via two complementary decay processes at rates $\Gamma_{1\rightarrow 3} = \Gamma_{3\rightarrow 1} \equiv \Gamma_g$. The two excited states 2 and 4 are connected via similar rates $\Gamma_{2\rightarrow 4} = \Gamma_{4\rightarrow 2} \equiv \Gamma_e$. These incoherent spin flips are induced by interaction with the phonon bath. All six incoherent processes can be described by a jump evolution and are associated with quantum noise on account of the (quantum) fluctuation-dissipation theorem.

The full 4×4 density matrix evolves as

$$\frac{d}{dt}\hat{\rho} = \mathcal{L}\hat{\rho}, \tag{6.37}$$

where $\mathcal{L}$ is the Liouville superoperator which we introduced in Sect. 6.1.2. $\mathcal{L}$ naturally separates into one contribution from each coupling or decay channel. Coherent coupling between two levels $i \leftrightarrow j$ leads to a Rabi oscillation between the populations $\hat{\rho}_{ii}$ and $\hat{\rho}_{jj}$ and coherence $\hat{\rho}_{ij}$ (and $\hat{\rho}^*_{ji}$) between these levels. This evolution, which would be reversible if it was the only coupling process, is described by:

$$\mathcal{L}_{coh,i\leftrightarrow j}\hat{\rho} = \frac{1}{i\hbar}[\hat{H}_{i\leftrightarrow j}, \hat{\rho}], \tag{6.38}$$

with

$$\mathcal{L}_{coh,i\leftrightarrow j} = i\frac{\Omega_{ij}}{2}(\mid j\rangle\langle i \mid \hat{\rho}+ \mid i\rangle\langle j \mid \hat{\rho} - \hat{\rho} \mid j\rangle\langle i \mid -\hat{\rho} \mid i\rangle\langle j \mid) \tag{6.39}$$

with Ω_{ij} being the Rabi frequency.

Incoherent population decay from level j to i is an irreversible process associated with a coupling to a large reservoir (often referred to as the *bath*). It results in a one-way exponential decay that can be represented by the Liouville operator $\mathcal{L}_{inc,j\leftrightarrow i}$ (see Sect. 6.1.2):

$$\mathcal{L}_{inc,j\leftrightarrow i} = \frac{\Gamma_{j\to i}}{2}(2 \mid i\rangle\langle j \mid \hat{\rho} \mid j\rangle\langle i \mid -\hat{\rho} \mid j\rangle\langle j \mid - \mid j\rangle\langle j \mid \hat{\rho}), \tag{6.40}$$

$\Gamma_{j\to i}$ being the incoherent population decay rate.

The four-level model presented here differs from other model definitions [158]. However, the method presented applies to any of these models.

6.3.2 Separation of time scales

As introduced in Sect. 6.2 [133] we distinguish the various terms in $\mathcal{L}$ into large and small terms, corresponding to a rapid and a slow evolution. The coupling between the spin-up states 1 and 2 and the coupling between the spin-down states 3 and 4 are generally strong compared to the coupling between the two ground states 1 and 3 and the coupling between the two excited states 2 and 4. In Fig. 6.1 this corresponds to vertical transitions for the strong couplings and horizontal transitions for the weak coupling. The Rabi frequencies Ω_e and Ω_g are linear in the coupling matrix elements which allows to treat them as first-order terms in a smallness parameter. However, the rates Γ_e and Γ_g are quadratic in the coupling matrix and can therewith be treated as second order terms. The quadratic coupling follows from Fermi's golden rule. Given these distinctions we can separate the Liouville operator into three terms:

$$\mathcal{L} = \mathcal{L}_0 + \mathcal{L}_1 + \mathcal{L}_2 \tag{6.41}$$

where $\mathcal{L}_0$ is the zero-order operator and contains the matrix elements δ_i, Γ_0 and $\Omega_\pm$. $\mathcal{L}_1$ describes the first-order contributions of the Rabi frequencies Ω_g and Ω_e. And $\mathcal{L}_2$ contains the remaining contributions Γ_g and Γ_e of second-order contribution.

In analogy to the line of argumentation in Sect. 6.2, $\mathcal{L}_0$ drives the system to a quasisteady state on a rapid time scale. This happens before the slow terms $\mathcal{L}_1$ and $\mathcal{L}_2$ have had time to cause noticeable change. Since the operator

$\mathcal{L}_0$ does not couple the spin-up states 1 and 2 to the spin-down states 3 and 4, the parameters determining the quasisteady state are the total population $n_+(t) = \rho_{11}(t) + \rho_{22}(t)$ of the spin-up states and $n_-(t) = \rho_{33}(t) + \rho_{44}(t)$ of the spin-down states. On the long time scale, the operators $\mathcal{L}_1$ and $\mathcal{L}_2$ mix the spin-up states and the spin-down states, so that the populations n_+ and n_- can change. This causes a slow evolution of the system through the subspace of steady states with respect to $\mathcal{L}_0$.
The projection operator, $\hat{\mathcal{P}}$, onto the quasisteady states satisfies $\mathcal{L}_0\hat{\mathcal{P}} = \hat{\mathcal{P}}\mathcal{L}_0 = 0$ (see Sect. 6.2). Consequently, the evolution of $\hat{\mathcal{P}}\hat{\rho}$ occurs exclusively on the slow time scale, determined by $\mathcal{L}_1$ and $\mathcal{L}_2$. The complementary projection operator is $\hat{\mathcal{Q}} = 1 - \hat{\mathcal{P}}$, and the Liouville Eq. (6.37) can be separated (similar to the set of coupled Eq. (6.26) and (6.27) into:

$$\frac{d}{dt}\hat{\mathcal{P}}\hat{\rho} = \hat{\mathcal{P}}(\mathcal{L}_1 + \mathcal{L}_2)\hat{\mathcal{P}}\hat{\rho} + \hat{\mathcal{P}}(\mathcal{L}_1 + \mathcal{L}_2)\hat{\mathcal{Q}}\hat{\rho}. \tag{6.42}$$

$$\frac{d}{dt}\hat{\mathcal{Q}}\hat{\rho} = \hat{\mathcal{Q}}(\mathcal{L}_1 + \mathcal{L}_2)\hat{\mathcal{P}}\hat{\rho} + \hat{\mathcal{Q}}\mathcal{L}\hat{\mathcal{Q}}\hat{\rho}. \tag{6.43}$$

In order to get an equation for $\hat{\mathcal{P}}\hat{\rho}$ alone, we eliminate $\hat{\mathcal{Q}}\hat{\rho}$ in the same way as presented in Eq. (6.28) to (6.35). By restricting the result to second order, we get an expression for the time evolution of the projection $\hat{\mathcal{P}}\hat{\rho}$

$$\frac{d}{dt}\hat{\mathcal{P}}\hat{\rho} = \hat{\mathcal{P}}(\mathcal{L}_1 + \mathcal{L}_2)\hat{\mathcal{P}}\hat{\rho} + \hat{\mathcal{P}}\mathcal{L}_1\int_0^\infty d\tau e^{\mathcal{L}_0\tau}\hat{\mathcal{Q}}\mathcal{L}_1\hat{\mathcal{P}}\hat{\rho}(t). \tag{6.44}$$

This formula can be used to calculate the slow spin dynamics.

Application to the four-level system

To separate the dominant (fast) evolution from the weaker (and slower) components we assume all spin-changing rates to be relatively small in comparison with the spontaneous lifetime of the excited state, in other words:
$\{\Gamma_g, \Gamma_e, \Omega_g, \Omega_e\} \ll \Gamma_0$. Additional, we distinguish between the weak-pumping limit where $\{\Omega_-, \Omega_+\} \ll \Gamma_0$ and the regime of moderate to strong optical excitation $\{\Omega_-, \Omega_+\} > \Gamma_0$. In the weak-pumping limit the two upper levels are barely excited and the level dynamics is dominated by the interaction between the two ground states. This case is analyzed in 6.3.3. The following discussions focuses on the regime of moderate to strong optical excitation.

For moderate to strong optical fields, the cycling dynamics in the two optical transitions will quickly exceed any spin transition rate and therefore enable the separation of three time scales. We have explained that in this case

the operator $\mathcal{L}_0$ describes the fast dynamics. As the optical transitions are spin conserving, the total spin-up population $n_+ = \hat{\rho}_{11} + \hat{\rho}_{22}$ and the total spin-down population $n_- = \hat{\rho}_{33} + \hat{\rho}_{44}$ are both invariant under operation of $\mathcal{L}_0$. The projection operator $\hat{\mathcal{P}}$ associated with $\mathcal{L}_0$ thus projects the density matrix in the two spin subspaces

$$\hat{\mathcal{P}}\hat{\rho}(t) = n_+(t)\bar{\hat{\rho}}_+ + n_-(t)\bar{\hat{\rho}}_-. \tag{6.45}$$

The two following submatrices describe the steady-state distributions within the spin-up and spin-down subspaces

$$\bar{\hat{\rho}}_\pm = \begin{pmatrix} (1-\alpha_\pm) & c_\pm \\ c_\pm^* & \alpha_\pm \end{pmatrix}, \tag{6.46}$$

We get a solution for the coefficients when solving the time-dependent Schrödinger equation in the rotating wave approximation:

$$\alpha_\pm = \frac{\Omega_\pm^2}{\Gamma_0^2 + 2\Omega_\pm^2 + (2\delta_\pm)^2}, \tag{6.47}$$

$$c_\pm = \frac{-2\delta_\pm - i\Gamma_0}{\Gamma_0^2 + 2\Omega_\pm^2 + (2\delta_\pm)^2}, \tag{6.48}$$

where $\alpha_\pm$ is the the excited-state fraction and $c_\pm$ the (complex) coherence. The frequency detunings are $\delta_+ = \delta_2$ and $\delta_- \equiv \delta_4 - \delta_3$ respectively.

Substituting the $\hat{\mathcal{P}}$ projection specified by Eq. (6.45) and (6.46) in the general Eq. (6.44) we get a solution for the dynamics of the spin populations $n_+(t)$ and $n_-(t)$. The result is a generic expression of the form

$$\frac{d}{dt}n_+(t) = -R_{+\to-}n_+(t) + R_{-\to+}(t) = -\frac{d}{dt}n_(t). \tag{6.49}$$

$R_{+\to-}$ is the jump rate from the spin-up to the spin-down manifold while $R_{-\to+}$ describes the reverse process. Explicit expressions for these jump rates are calculated through substitution of $\mathcal{L}_0$, $\mathcal{L}_1$ and $\mathcal{L}_2$ in the appropriate expressions as explained in Sect. 6.3.3

Equation (6.49) can be interpreted in terms of two population operators with eigenvalues $n_\pm = \{0, 1\}$ and quantum jumps between two spin manifolds. The jumps occur naturally and are driven by the internal population dynamics and quantum noise. Alternatively, one could stress the importance of quantum state projection through observation [151]. In this description, the optical cycling transitions within each manifold creates quantum entanglement between

the atomic spin state and the handedness of the optical emission, thus allowing one to extract information on the spin state by (projective) measurements on the optical field. This situation is similar to that found in intermittent fluorescence, where the optical measurement enables one to decide whether the atomic population is located in the optically active manifold or in the dark *shelving* state [145, 149].

Two contributions to the jump rates

The essential ingredient in our analysis is the separation of the 4×4 density matrix $\hat{\rho}$ into four blocks of 2×2 elements that combine kets and bras with the same spin combinations. The action of the superoperators $\mathcal{L}_1$ and $\mathcal{L}_2$ on these blocks is quite different. The operator $\mathcal{L}_1$, associated with coherent coupling at Rabi frequencies Ω_g and Ω_e, only transfers elements from the diagonal blocks to the off-diagonal blocks of $\hat{\rho}$ and vice versa. As a result of this blocklike operation the term $\hat{\mathcal{P}}\mathcal{L}_1\hat{\mathcal{P}}\hat{\rho} = 0$ in Eq. (6.44). Operator $\mathcal{L}_2$, associated with incoherent spin flips at rates Γ_g and Γ_e, mixes elements within each block and only transfers elements between the diagonal blocks.

Furthermore, the quantum jump rates $R = R_{coh} + R_{inc}$ separate into a *coherent* R_{coh} and an *incoherent* R_{inc} contribution. R_{coh} is associated with $\mathcal{L}_1$ while R_{inc} is associated with $\mathcal{L}_2$.

The incoherent contribution to the jump rates are easily calculated as

$$R_{inc,+\to-} = (1 - \alpha_+)\Gamma_g + \alpha_+\Gamma_e \tag{6.50}$$

$$R_{inc,-\to+} = (1 - \alpha_-)\Gamma_g + \alpha_-\Gamma_e \tag{6.51}$$

They are the averages of the spin flip rates between the ground and excited state weighted over the relative excited state populations $\alpha_\pm$. A calculation of the coherent contributions R_{coh} is more complicated and will be dealt with in the next section.

6.3.3 Jump rate due to coherent spin coupling

General remarks

Calculating the jump rate induced by coherent spin coupling is carried out using Mathematica. The blocklike operations of the superoperators introduced before eases the evaluation of the complicated second term in Eq. (6.44). The evaluation is done in three steps. Starting from the diagonal matrix $\hat{\mathcal{P}}\hat{\rho}$ on the right-hand site

(i) operation $\mathcal{L}_1$ transfers coherence to the off-diagonal blocks

(ii) integral operation modifies the off-diagonal blocks elements

(iii) operation $\hat{\mathcal{P}}\mathcal{L}_1$ brings these elements back to the on-diagonal blocks where they contribute to the evolution of the spin populations n_+ and n_-.

The integral operation (ii) is the most complicated step. It involves the inversion of the 4×4 matrix that describes the dynamics in the 2×2 off-diagonal block. The following special cases are discussed

(i) a frequency-degenerate system ($\delta_2 = \delta_3 = \delta_4 = 0$) under various forms of excitation

(ii) the same system in the weak-pumping limit

(iii) a detuned system with $\delta_3 \neq 0$ and $\delta_2, \delta_4 \ll \Gamma_0$

Jump rate in a frequency-degenerate system

The first case we analyze is the frequency-degenerate system where $\delta_2 = \delta_3 = \delta_4 = 0$. Applying the three-step procedure introduced in the previous section results in the following expression describing the coherent jump rate from the two spin-up to the two spin-down levels

$$R_{coh,+\to-} = \frac{2\Gamma_0^5\Omega_g^2 + \Gamma_0^3(\Omega_+^2 + \Omega_-^2)\Omega_g^2 + 2\Gamma_0\Omega_+^2(\Omega_-\Omega_g + \Omega_+\Omega_e)^2}{(\Gamma_0^2 + 2\Omega_+^2)[2\Gamma_0^2(\Omega_+^2 + \Omega_-^2) + (\Omega_+^2 - \Omega_-^2)^2]} \tag{6.52}$$

with the assumption $\Gamma_g, \Gamma_e \ll \Gamma_0$. For the reverse process the jump rate $R_{coh,-\to+}$ is described by a similar expression that only differs in its spin labels, which are now swapped by the transformation $+ \leftrightarrow -$.

Figure 6.2 shows three examples for the jump rate dependance on the optical intensity of linearly polarized light, expressed as $\Omega_+^2 = \Omega_-^2 = \Omega_0^2$. A strong power dependance of the jump rates due to the coherent and incoherent spin-changing processes is visible. The solid curve shows how the *incoherent* jump rate R_{inc} changes gradually from its weak-pumping value of Γ_g to its strong pumping value $(\Gamma_g + \Gamma_e)/2$ on account of the increased excited-state populations. The dashed (blue) and dashed-dotted (black) curves show the power dependence of the *coherent* jump rate R_{coh} for two different values of the coherent coupling frequencies $\Omega_g = \Omega_e$.

With linear polarized excitation Eq. (6.52) reduces to

$$R_{coh,+\to-} = R_{coh,-\to+} = \left(\frac{\Gamma_0}{2\Omega_0^2}\right)\left(\frac{(1+\beta)\Omega_g^2 + \beta^2(\Omega_g + \Omega_e)^2}{(1+2\beta)}\right), \tag{6.53}$$

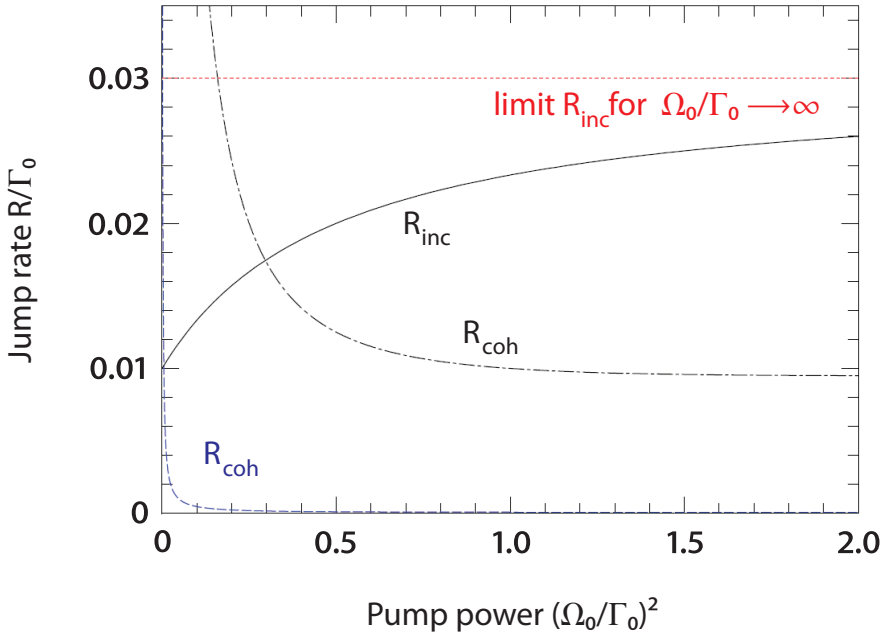

Figure 6.2: *Calculated jump rates* $R_{-\to+} = R_{+\to-}$ *as function of the optical intensity of linearly polarized light:* $\Omega_+^2 = \Omega_-^2 = \Omega_0^2$. *The solid curve shows how the jump rate* R_{inc} *due to incoherent spin flips changes gradually from its groundstate value of* Γ_g *to an average value of* $(\Gamma_g + \Gamma_e)/2$ *for saturated excitation (parameters:* $\Gamma_g = 0.01$, $\Gamma_e = 0.05$*). The two dashed curves shows the jump rate due to coherent spin coupling for* $\Omega_g = \Omega_e = 0.01$ *[dashed (blue) curve] and* $\Omega_g = \Omega_e = 0.1$ *[dashed dotter (black) curve]. All units are normalized to the spontaneous emission rate* Γ_0. *Note the pronounced decrease in* R_{coh} *at larger pump rates and the divergence for* $\Omega_0 \to 0$. *This divergence can be removed by including other decay and coupling processes into the description (see Fig. 6.4).*

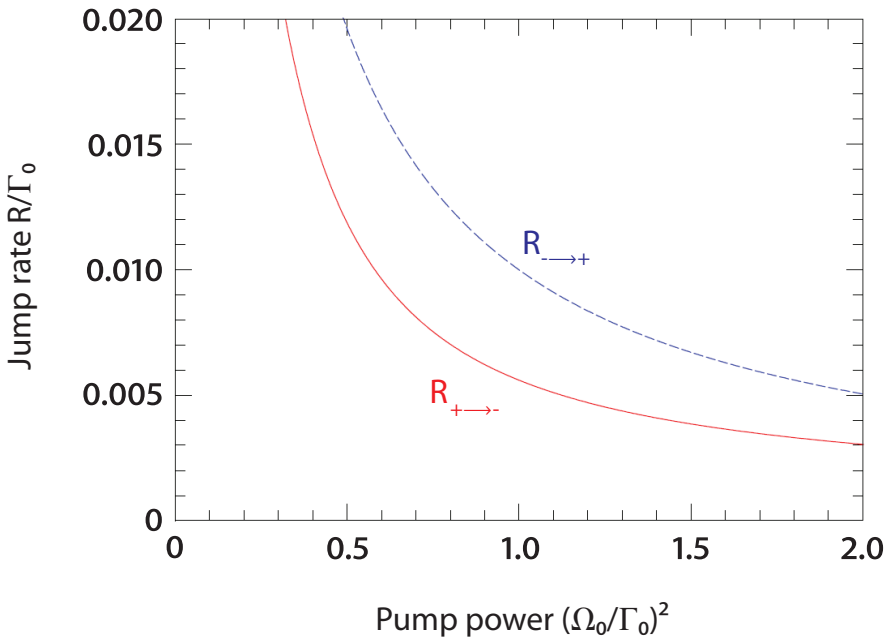

Figure 6.3: *Coherent jump rates R_{coh} under circularly polarized excitation. The jump rates due to coherent spin coupling are calculated as function of the intensity of right-handed circularly polarized light, expressed as Ω_+^2 ($\Omega_- = 0$). The two curves show the jump rate $R_{coh,+\to-}$ from the spin up to the spin-down manifold [solid (red) curve] and the jump rate $R_{coh,-\to+}$ for the reverse jumps [dashed (blue) curve] for $\Omega_g = \Omega_e = 0.1$, $\Gamma_g = \Gamma_e = 0.01$, and $\delta_3 = 0$. All units are normalized to Γ_0. The resulting unbalance in spin population depends on the ratio of the two depicted jump rates R_{coh} and the jump rate R_{inc} associated with incoherent spin flips.*

with $\beta \equiv (\Omega_0/\Gamma_0)^2 \propto I/I_{sat}$ measuring the degree of saturation. This jump rate diverges in the weak-pumping limit and decreases to a limiting value $(\Omega_g + \Omega_e)^2/(2\Gamma_0)$ for strong pumping.

Figure 6.3 shows a typical example of the power dependence of the jump rates R_{coh} under excitation with righthanded circularly polarized light ($\Omega_- = 0$). Optical excitation with circularly polarized light leads to an unbalance between the two jump rates

$$R_{coh,+\to-} = \frac{\Gamma_0}{1 + 2\Omega_+^2/\Gamma_0^2}\left[\frac{\Omega_g^2}{\Omega_+^2} + \frac{\Omega_+^2\Omega_e^2}{\Gamma_0^2(\Gamma_0^2 + \Omega_+^2/2)}\right], \tag{6.54}$$

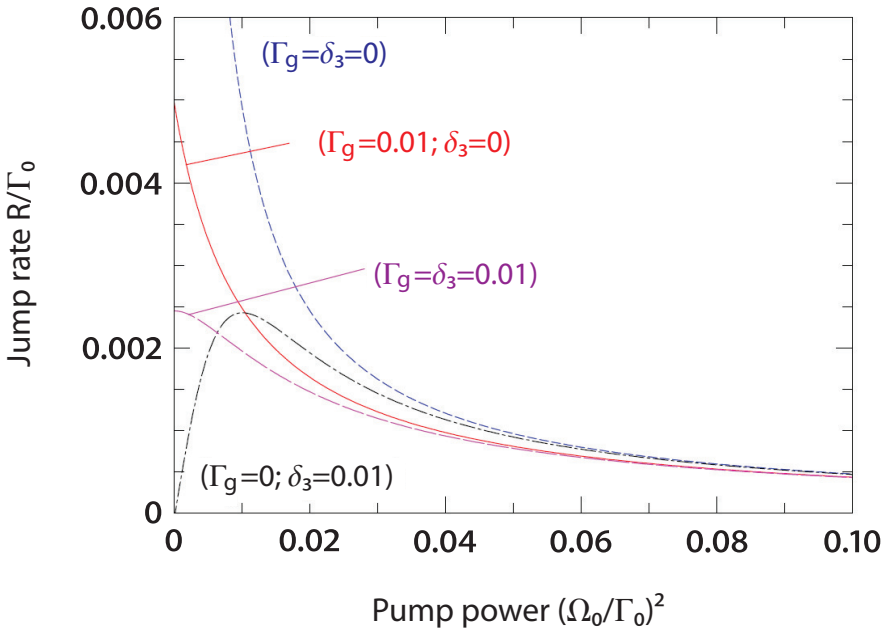

Figure 6.4: *Calculated jump rate $R_{-\to+} = R_{+\to-}$ due to coherent spin coupling as function of the optical intensity of linearly polarized light, expressed as $\Omega_+^2 = \Omega_-^2 = \Omega_0^2$. The dashed (blue) curve is a zoom in of a similar result depicted in Fig. 6.2 for $\Omega_g = \Omega_e = 0.01$. The other three curves show how the divergence at low pump rate can be removed by inclusion of other decay processes in the description. We have included only spin flips [solid (red) curves with either $\Gamma_g = 0.01$ or $\delta_3 = 0$], and both (dotted) (pink) curve with $\Gamma_g = \delta_3 = 0.01$). All units are normalized to Γ_0.*

$$R_{coh,-\to+} = \frac{\Omega_g^2}{\Omega_+^2}\Gamma_0. \tag{6.55}$$

This visible unbalance is shown in Fig. 6.4. The graph shows curves for an intrinsically *balanced* system with equal ground- and excited-state spin dynamics at $\Omega_g = \Omega_e = 0.1\Gamma_0$ and $\Gamma_g = \Gamma_e = 0.01\Gamma_0$. The difference between the two jump rates can be more pronounced in an *unbalanced* system. The mentioned difference will result in optical pumping from one spin manifold to the other and in an unbalance of the steady-state spin population ($\bar{n}_+ \neq \bar{n}_-$, as determined by the balance $R_{+\to-}\bar{n}_+ = R_{-\to+}\bar{n}_-$ with $R = R_{coh} + R_{inc}$).

Weak-pumping limit and the quantum Zeno effect

The weak-pumping limit ($\Omega_-, \Omega_+ \ll \Gamma_0$) of Eq. (6.52) simplifies to

$$R_{coh,+\to-} \approx \left(\frac{\Omega_g^2}{\Omega_+^2 + \Omega_-^2} \right) \Gamma_0, \tag{6.56}$$

when also assuming $\Omega_e/\Omega_g \ll (\Omega_+/\Gamma_0)^2$. This jump rate diverges at zero pumping. The corresponding monotone decrease at increased pumping is a manifestation of the quantum Zeno effect [159]. It shows how repeated inspection of a quantum state and the resulting state projection slow down the naturally oscillatory evolution associated with coherent coupling. Repeated inspection goes unnoticed for the incoherent spin flip process, as the exponential decay associated with this process starts off linearly, whereas the coherent evolution starts off quadratically in time.

The divergence of the coherent spin jump in the weak-pumping limit is caused by a similar divergence in the lifetime of the ground-state coherence $\hat{\rho}_{13}$ under $\mathcal{L}_0$ evolution only. This divergence can be tentatively removed by incorporating the ground-state spin flip process at a rate Γ_g into the description. This can be done through modification of the exponent in the integrand of Eq. (6.44) from $e^{\mathcal{L}_0\tau}$ to $e^{(\mathcal{L}_0+\mathcal{L}_2)\tau}$. This changes Eq. (6.56) to

$$R_{coh,+\to-} \approx \frac{\Omega_g^2}{2\Gamma_g'}, \tag{6.57}$$

with the total decay rate of the ground-state coherence

$$\Gamma_g' = \Gamma_g + \frac{\Omega_+^2 + \Omega_-^2}{2\Gamma_0} \tag{6.58}$$

combining the natural incoherent spin flip rate Γ_g with an extra pump-induced decoherence rate $\Gamma_{extra} = \left(\Omega_-^2 + \Omega_+^2\right) / (2\Gamma_0)$. For three-level systems, a similar extension with part of the slow dynamics changes the general expressions for the jump rate in three-level systems derived by Nienhuis [160] into the more specific expressions discussed by Kimble et al. [149].

Jump rate at frequency detuning

Finally, we extend our four-level model to the general case by including the frequency detunings δ_2,δ_3 and δ_4. These detunings are easily incorporated in the $\mathcal{L}_0$ and the associated steady-state distributions $\hat{\rho}_+$ and $\hat{\rho}_-$ given by Eq. (6.46) to (6.48). Substituting the modified $\mathcal{L}_0$ with the original $\mathcal{L}_1$ and

$\mathcal{L}_2$ in the generic Eq. (6.44) again yields expressions for the *coherent* jump rates R_{coh}. The following results are for the case of limited optical detuning where $\delta_2, \delta_4 \ll \Gamma_0$. However the full evolution of the ground-state coherence is taken into account including the spin flip rate Γ_g and a possible ground-state detuning $\delta_3 \neq 0$ in the evolution $exp(\mathcal{L}_0 + \mathcal{L}_2)\tau$. The results is an extension of Eq. (6.52) to

$$R_{coh,+\to-} = Re\left(\frac{2\Gamma_0^5\Omega_g^2 + \Gamma_0^3(\Omega_+^2+\Omega_-^2)\Omega_g^2 + 2\Gamma_0\Omega_+^2(\Omega_-\Omega_g + \Omega_+\Omega_e)^2}{(\Gamma_0^2+2\Omega_+^2)\left[2\Gamma_0^2(\Omega_+^2+\Omega_-^2+2\Gamma_0\{\Gamma_g+i\delta_3\}) + (\Omega_+^2-\Omega_-^2)^2\right]}\right). \tag{6.59}$$

The spin flip rate Γ_g and the ground-state detuning δ_3 have comparable effects. Both modify the built up of ground-state coherence that is the first step toward a coherently driven spin change. These effects are only visible at relatively weak pumping ($\Omega_+^2 + \Omega_-^2 < 2\Gamma_0\sqrt{\Gamma_g^2+\delta_3^2}$).

Fig. 6.4 shows how the divergence in the calculated jump rate is removed both for a finite spin flip rate Γ_g and a finite ground-state detuning δ_3. The curves shown are based on Eq. (6.59). In case of the weak-pumping limit, this equation predicts a limiting jump rate $R_{coh,+\to-} \approx Re\{\Gamma_g^2/[2(\Gamma_g + i\delta_3)]\}$. For the frequency-degenerate system ($\delta_3 = 0$), this limit is $\Gamma_g^2/(2\Gamma_g)$. For the frequency-detuned system this limiting value is lower. At a sufficiently large frequency detuning ($\delta_3 \gg \Gamma_g$) the jump rate becomes practically zero in the weak-pumping limit, when none of the other interactions is strong enough to overcome the dominant frequency splitting δ_3.

6.3.4 Experimental possibilities

Quantum jumps in the spin state should be observable as jumps in any spin-dependent observable such as the measured Faraday [143] of Kerr effect [144], or the (polarization of the) spontaneous emission [139]. Most of these observables, however, provide only a weak measurement of the spin state. At a typical Faraday rotation angle of less than 1mrad [143] more than 10^6 photons are needed to measure the spin state with sufficient certainty, making it practically impossible to observe the predicted quantum jumps by Faraday rotation.

As mentioned before, monitoring the corresponding changes in the reflectivity of an encompassing optical cavity as suggested in this thesis could be used to search for spin quantum jumps. The reflectivity of such a system could potentially change from 0 to $\sim 100\%$ upon a spin flip [54]. Such a measurement can be very efficient. It thereby presents a strong quantum measurement

that projects the spin system onto an eigenstate. Changes in the cavity reflectivity from 0 to 50% due to the presence or absence of an optical transition have already been observed experimentally for a single InAs quantum dot in a high-finesse GaAs/AlGaAs cavity [55]. In Chap. 4 we demonstrated how to fabricate and modify cavities to make them polarization degenerate, the prerequisite to observe reflection of up to 100%. Initial results will be presented in Chap. 8. Potentially the results allow for an almost direct measurement of the spin state through the simple observation of the presence or absence of reflected photons of a specific polarization.

Different inspection technique are conceivable. They have in common that the jump dynamics would be extracted from a statistical analysis of the time dependence of the spin-sensitive inspection channels $I_+(t)$ and $I_-(t)$. As for the proposed reflectivity measurement, these inspection channels are just the reflected intensities of the two circular polarizations. Typical quantities to measure are correlation functions such as

$$C_{\pm\pm}(\Delta t) \equiv \langle I_\pm(t) I_\pm(t+\Delta t)\rangle_t \tag{6.60}$$

where the brackets $\langle\rangle_t$ denote averaging over time. These correlation functions obey the same time evolution as the associated populations [151]. They generally decay exponentially at precisely the jump rates that are to be determined [161]. The modulation contrast of these correlation functions is linked to the criterium of strong versus weak measurements mentioned above.

6.4 Conclusion

In summary, we have described a model that analyzes the spin dynamics of a four-level system. Using the approach of the separation of time scales between the fast spin-conserving optical transitions and slower spin-changing transitions, the occurrence of sudden quantum jumps between spin-up and spin-down states under optical inspection are predicted. A natural interpretation of these jumps is as follows: The optical interaction first creates quantum entanglement between the atomic spin state and the optical polarization or emission direction of the interacting photon. A consecutive measurement on the photon will then project both the photon state and the spin state onto an eigenstate of the measurement operator. In the discussion a distinction between quantum jump due to incoherent spin flips and coherent spin coupling has been made. Derived expressions for both phenomena are presented and the physical consequences are discussed. One example thereof is the quantum zero

effect, where repetitive measurements and projections are predicted to reduce the jump rate associated with coherent spin coupling.

6.5 Further extension of the model

A more complicated four-level system model could include the back action of the electron spin on either the intracavity field or the nuclear spins. As a result of the backaction of the spin state on the intracavity optical field, this intracavity field will also perform jumps even if the injected field is constant. One approach to deal with this complication is to analyze the jump dynamics for two different but fixed states of the intracavity field, each one being associated with a different spin state of the quantum dot. If the cavity operates in the Purcell regime, the strong ac Stark shift will push the intracavity mode with the matched handedness out of resonance, thereby forcing the intracavity field to be circularly polarized in the handedness that has least interaction with the occupied spin state. This handedness is expected to switch abruptly (within the optical lifetime of the cavity) upon a quantum jump of the other spin state. A second and more rigorous approach to include the back action from the spin state on the intracavity field could be based on a rederivation of the state-selectivity reflectivity. This is discussed in paper [54] for a two-level system instead of a four-level one. This quantum-mechanical treatment would be a generalization of the so-called Maxwell-Bloch equations. It should result in an input-output formalism for the optical field operators in and outside a filled cavity [162]. For optical cavities with extremely large finesses, such that the cavity loss rate $\kappa \ll \Gamma_0$, other intriguing phenomena such as lasing of a single quantum dot have been predicted [163]. A final extension of the model could include the effect of dynamical nuclear spin polarization. This backaction effect leads to a build up of the nuclear magnetic field felt by the electron and causes the resonance frequencies to shift, and in certain cases lock to the driving frequencies.